Electron Diffraction of Molecules in Specific Quantum States: A Theoretical Study of Vibronically Excited *s*-Tetrazine

Seol Ryu,[†] Richard M. Stratt,[†] Kyoung K. Baeck,[‡] and Peter M. Weber*,[†]

Department of Chemistry, Brown University, Providence, Rhode Island 02912, and Department of Chemistry, Kangnung National University, Kangnung 210-702, Korea

Received: September 10, 2003; In Final Form: December 3, 2003

The electron diffraction patterns of *s*-tetrazine ($C_2N_4H_2$) in specific electronic and vibrational states have been calculated for isotropic samples, for molecules that are aligned in high-intensity laser fields, and for orientationally clamped molecules. Using structures and normal mode displacement coordinates from a coupled-cluster ab initio calculation, we evaluate diffraction patterns of the molecule in the vibrationless level of S_0, and the 0^0, 1^2, $6a^3$, and $16a^8$ vibrational levels of the S_1 state. It was found that both the electronic and the vibrational excitations lead to changes in the diffraction patterns of isotropic samples in the range of ±1%. Effects of the respective orientation of the excitation laser polarization and the detector direction are clearly observed. Alignment of the molecule in intense laser fields, with intensities ranging from 1.06 to 9.56 TW/cm^2, provides for an increase in the modulation depths of all diffraction patterns and can be used to further enhance the observability of vibrational diffraction patterns. This study demonstrates that vibrational probability density distributions should be observable using electron diffraction and that skillful orientation of the excitation laser polarization, the polarization of the alignment laser, and the direction of signal detection can be exploited to map the wave functions from different sides. The differences in diffraction patterns of nominally isoenergetic vibrational states provide an opportunity for experimentally observing the flow of vibrational energy through the phase space by time-dependent three-dimensional mapping of the wave packet.

I. Introduction

Pump−probe diffraction experiments are receiving increasing attention as tools to observe directly the structural dynamics of molecules during chemical reactions.[1−3] In a typical experiment, a short laser pulse prepares the molecule in an excited state, from where the dynamical process of interest ensues. A short burst of electrons or X-rays is diffracted off the molecular sample, and the dependence of the diffraction pattern on the time delay between the pump laser pulse and the probe pulse is observed. The transformation from the space of the scattering vector to the real space of molecular distances provides the time-dependent molecular structure.

Dynamical processes of isolated molecular systems can be thought of in terms of time-evolving wave packets, which are comprised of electronic, vibrational, and/or rotational states. In condensed phases, additional degrees of freedom include the solute−solvent and solvent−solvent motions. To the extent that such dynamical processes result from the superpositions of many (possibly an infinite number) of time-dependent wave functions, an important question is the limit of observability of individual excited-state wave functions. In other words, if a system is prepared in an individual excited state, can the effect of this excitation be observed using a diffraction experiment? While exploring this question, we discovered the exciting possibility of performing a tomography of quantum mechanical probability density distributions by using different geometries of the excitation laser polarization, the direction of the electron beam, and the direction of the scattered radiation.[4] We also found that the mapping of the probability density distributions are greatly aided by the use of an "optical goniometer", which utilizes high-intensity laser fields to align molecules in specific directions.[5] The present paper describes these discoveries.

Studies of diffraction patterns of systems in specific quantum states have been performed before: Böwering et al. explored the consequences of preparing molecules in pure rotational states;[6] Ben-Nun et al. discussed the effect of electronic excitation of atoms on the X-ray and electron scattering factors;[7] and Geiser and Weber examined the consequence of vibrational excitation in diatomic molecules clamped in a specific position.[8] The latter work has been extended to a triatomic molecule with isotropic orientations, where specific vibrations are prepared by a two-photon excitation with a polarized laser beam.[4] Ewbank and co-workers have also modeled the diffraction signatures of some vibrationally excited diatomics resulting from photodissociation.[9]

The objective of the present work is to extend the previous studies in two ways. First, we move from the diatomic and triatomic molecules studied previously to a polyatomic model system. And, second, we investigate molecules with both isotropic orientational distributions and with specific alignments. As a model system we chose *s*-tetrazine, $C_2N_4H_2$. With eight atoms and an aromatic ring, this molecule can truly represent polyatomic systems, yet it is small enough to allow a detailed vibronic analysis of excited-state spectra.[10,11] *s*-Tetrazine features a rich set of vibrational motions, including ring breathing, puckering, bending, and stretching vibrations, which can be selectively prepared by tunable laser beams.

The theoretical simulations of the diffraction patterns reflect a situation where a laser pulse prepares isolated *s*-tetrazine molecules in the S_1 electronic state. The bandwidth of the laser is taken to be small enough for individual vibronic states to be

[†] Brown University.
[‡] Kangnung National University.

10.1021/jp031061x CCC: $27.50
Published on Web 01/24/2004

excited. Moreover, we assume that the distribution of rotational states of the molecules before the excitation step is mapped onto the excited-state surface, without further consideration of time-dependent rotational wave packets. This situation can be implemented in the laboratory by exciting the Q-branch of a vibronic transition and probing the diffraction pattern before the rotational states dephase.

It is well-known that *s*-tetrazine excited to the S_1 state experiences an internal conversion to the S_0 surface on the 500 ps time scale[12] and that thereafter it breaks apart to 2HCN + N_2 in a concerted triple dissociation.[13,14] Those dynamical processes, while inherently interesting, are ignored in the present calculation, as the molecule is stable on the picosecond time scale that is relevant for the situation explored in the present paper.

As was pointed out in a recent study, the diffraction patterns of perfectly oriented molecular systems are fully modulated.[5] However, the isotropic orientation of molecules in typical gas-phase samples reduces the modulation depth to only about 1% of the total signal. This makes gas-phase diffraction patterns difficult to observe and analyze for many molecules with low symmetry. We showed that some of the modulation depth can be recovered by aligning the sample using intense laser fields as an optical goniometer.[5] While the laser fields required for alignment are high, typically in the terawatt per square centimeter range, they are within the reach of present-day pulsed lasers. The present paper therefore includes calculations of diffraction patterns of vibronically excited molecules that are aligned by high-intensity laser fields.

This paper is structured as follows. We first detail the ab initio calculations that provide us with a consistent set of molecular parameters for the *s*-tetrazine molecule. In subsequent sections we describe the simulation of the diffraction signals and then briefly review the implementation of the molecular alignment. Results and Discussion presents electron diffraction patterns for excitation to different vibronic states and for various geometries of the photoexcitation laser and the alignment laser. As will be seen, the effects of vibronic excitation are well within the range that can be probed with existing pump−probe diffraction instruments.

II. Theoretical Methods

A. Ab Initio Calculations. Selected structural parameters as well as some normal mode frequencies and coordinates are available for tetrazine in both the S_0 and the S_1 electronic states.[10,11,13,15] However, a complete set of normal mode coordinates is not readily available. To derive a consistent set of data, we performed ab initio calculations of both the S_0 and the S_1 electronic states and used those values even in cases where experimental or other theoretical data are available.

We chose the coupled-cluster singles and doubles (CCSD) and the equation of motion coupled-cluster singles and doubles (EOM-CCSD) methods of the ACES II program system,[16] for the ground-state S_0 and the excited-state S_1 calculations, respectively. To increase the speed of the CCSD calculations, the drop-MO technique (which should have minimal effects on the molecular properties of interest)[17] was used to freeze the six innermost core and six outermost virtual molecular orbitals of *s*-tetrazine.

The molecular structures were optimized with Dunning's double-ζ basis[18] plus polarization functions (DZP) with exponents $\zeta_H(p) = 0.7105$, $\zeta_C(d) = 0.6540$, and $\zeta_N(d) = 0.9020$.[19] All six Cartesian d-functions were used. The harmonic vibrational frequencies and coordinates were calculated by diagonalizing the force constant matrix obtained by finite difference from analytically computed gradients at the optimized structures. Table 1 provides the equilibrium bond lengths and angles for both the electronic ground-state S_0 and the S_1 excited electronic state. The calculated values agree well with the experimental values of Job and Innes,[20] which are also listed in Table 1. The quality of our results is similar to those with a DZP basis:[15] the vibrational frequencies are within 1% for S_0 and within 3% for S_1, except for the S_1-6b mode.[21] The small difference can be mainly attributed to drop-MO effects.[17] Since our main concern here is to provide a systematic set of parameters to calculate the diffraction signals, no further efforts were made to adjust the theoretical procedure to approach the experimental values more closely.

TABLE 1: Equilibrium Geometries of the Ground S_0 and the Excited S_1 States, Both of D_{2h} Symmetry, Obtained by CCSD Method (EOM-CCSD for S_1) with a DZP Basis Set, along with the Experimental Values of Reference 20[a]

parameter	CCSD+DZP	expt.
$\tilde{X}^1A_g$ (S_0)		
r_{CH}	1.0887	1.0726
r_{CN}	1.3463	1.3405
r_{NN}	1.3271	1.3256
θ_{NCN}	126.8	126.4
$\tilde{A}^1B_{3u}$ (S_1)		
r_{CH}	1.0868	1.063
r_{CN}	1.3404	1.324
r_{NN}	1.3241	1.349
θ_{NCN}	121.5	123.2

[a] Bond lengths are in angstroms, and angles are in degrees.

We investigated the diffraction signatures of vibrational states 1^2, $6a^3$, and $16a^8$ in the S_1 electronic state. Those states were chosen because the vibrations are vibronically active in the $S_0 \rightarrow S_1$ transition and because these particular overtones have similar energies (2008−2109 cm^{-1}). The normal mode displacements of these vibrations are listed in Table 2 and illustrated in Figure 1. Vibrations 1 and 6a are in-plane vibrations, while 16a is an out-of-plane ring deformation vibration. The change in the geometrical structure upon excitation from S_0 to S_1 is largely confined to a change of the NCN angle, causing significant vibronic activity in the coordinates of vibrations 1 and 6a.[11] Vibronic activity in the even quantum numbers of 16a results from a change in the curvature of the out-of-plane potential upon electronic excitation.

B. Diffraction Signals of Specific Vibronic States. In a previous publication we have developed a theoretical framework to describe diffraction signals from molecules in specific vibronic states.[4] Briefly, the total scattering intensity for a perfectly oriented N-atom molecule in a well-defined excited vibrational eigenstate is, within the first Born approximation, given as

$$I_{total}(s,\alpha,\Omega) = I_{atomic}(s) + I_{mol}(s,\alpha,\Omega) \qquad (1)$$

where the total scattered intensity I_{total} depends on the magnitude of the momentum transfer vector **s**, which is the difference between the final and the initial electron momentum, $\mathbf{s} = \mathbf{k} - \mathbf{k}_0$. In addition, the scattered intensity depends on the angle α at which the signal is observed, and the Euler angle $\Omega = (\theta,\varphi,\chi)$ that specifies the orientation of a molecule. All the angles are defined in Figure 2. As for eq 1, the total scattering is comprised of the atomic scattering I_{atomic}, which depends only on the magnitude of the momentum transfer, and the molecular scattering, I_{mol}, which depends on the momentum transfer as well as the angles α and Ω. The atomic and the molecular

TABLE 2: Three Harmonic Vibrational Frequencies and Their Associated Normal-Mode Eigenvectors $(\mathbf{e}^T)_{j\mu,\gamma}$ at the Equilibrium Geometry of the Excited S_1 State (As Obtained by the EOM-CCSD Method with DZP Basis Set)[a]

		a_g modes		a_u mode
		q_1	q_{6a}	q_{16a}
atom	direction	1064.1 cm^{-1}	731.2 cm^{-1}	253.4 cm^{-1}
C1	x	0.000	0.000	0.000
	y	0.000	0.000	0.000
	z	−0.451	−0.442	0.000
C2	x	0.000	0.000	0.000
	y	0.000	0.000	0.000
	z	0.451	0.442	0.000
H1	x	0.000	0.000	0.000
	y	0.000	0.000	0.000
	z	−0.145	−0.131	0.000
H2	x	0.000	0.000	0.000
	y	0.000	0.000	0.000
	z	0.145	0.131	0.000
N1	x	0.000	0.000	0.500
	y	0.294	−0.379	0.000
	z	−0.227	−0.009	0.000
N2	x	0.000	0.000	−0.500
	y	−0.294	0.379	0.000
	z	−0.227	−0.009	0.000
N3	x	0.000	0.000	0.500
	y	−0.294	0.379	0.000
	z	0.227	0.009	0.000
N4	x	0.000	0.000	−0.500
	y	0.294	−0.379	0.000
	z	0.227	0.009	0.000

[a] Here γ labels the modes, j the atoms, and μ the Cartesian directions in the molecular frame. The corresponding equilibrium atomic coordinates (in angstroms) are as follows: C_1 (0.000, 0.000, −1.317); C_2 (0.000, 0.000, 1.317); H_1 (0.000, 0.000, −2.404); H_2 (0.000, 0.000, 2.404); N_1 (0.000, 1.169, −0.662); N_2 (0.000, −1.169, −0.662); N_3 (0.000, −1.169, 0.662); N_4 (0.000, 1.169, 0.662). To obtain the matrix elements $(\mathbf{M}^T)_{j\mu,\gamma}$ in $amu^{-1/2}$, the dimensionless eigenvectors $(\mathbf{e}^T)_{j\mu,\gamma}$ need to be divided by the square roots of the masses of the associated atoms; i.e., $(\mathbf{M}^T)_{j\mu,\gamma} = (\mathbf{e}^T)_{j\mu,\gamma}/\sqrt{m_j}$ since the mass-weighted normal-mode coordinates q_γ are in $amu^{1/2}$ Å.

scattering signals are given by

$$I_{\text{atomic}}(s) = I_0\sigma_{\text{Ru}}(s)\sum_j |g_j|^2 \quad (2)$$

$$I_{\text{mol}}(s,\alpha,\Omega) = 2I_0\sigma_{\text{Ru}}(s)\sum_{j<k}\sigma_{jk}(s,\alpha,\Omega) \quad (j,k = 1, ..., N) \quad (3)$$

where I_0 is the intensity of the incident electron beam, and σ_{Ru} is the Rutherford scattering cross-section of an electron by a single charge.[22] The g_j are the complex atomic electron scattering factors,[23] which can be written in terms of an amplitude and a phase

$$g_j(s) = |g_j(s)|\, e^{i\eta_j}$$

We assume that the atomic scattering factor remains constant upon electronic and vibrational excitation. That is, as far as the structure factor is concerned, we invoke the independent atom approximation. While changes of the electron density distributions have indeed been shown to affect excited-state diffraction patterns,[7] those effects are typically observed at small diffraction angles. In contrast, the effect of the vibrational excitation is manifest at large diffraction angles.

The dependence of the diffraction pattern on the vibronic excitation enters through the molecular component, I_{mol}, which depends on the specific quantum state. In the subsequent discussion this is indicated as a subscript; for example, $I_{S_1,1^2}$ is

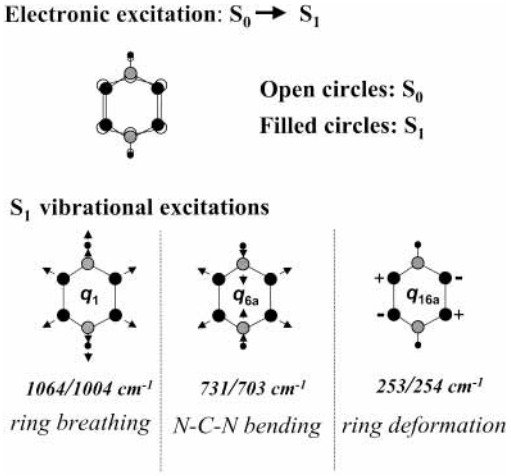

Figure 1. Top panel: the geometry change incurred by the *s*-tetrazine molecule, $C_2H_2N_4$, upon electronic excitation to the S_1 state. Bottom panel: the vibrational displacement vectors of vibrations 1, 6a, and 16a. The two vibrational frequencies shown for each mode are the harmonic frequencies calculated in this work and the experimental values, respectively.

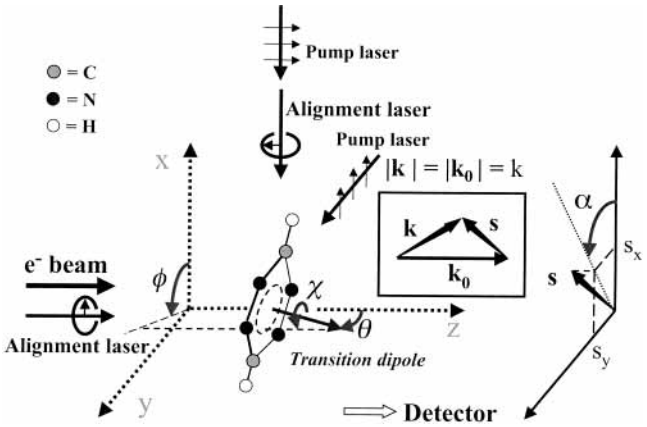

Figure 2. Geometry of the electron diffraction experiment. The electron beam propagates along the *z*-axis and intersects the molecule oriented at the Euler angles $\Omega = (\theta,\phi,\chi)$. The diffraction pattern is observed in the (x,y) plane. The pump laser that is used to excite to S_1 can either have an *x*-polarized or a *z*-polarized electric field vector, and the alignment laser is circularly polarized in either the (y,z) plane or the (x,y) plane.

the total (atomic + molecular) diffraction signal of the molecule in the S_1 state in vibration 1^2.

To calculate the eigenstate-dependent diffraction signal, we express the complete vibrational wave function as a product of one-dimensional wave functions,

$$|\psi\rangle = \prod_\gamma |\psi_\gamma(q_\gamma)\rangle$$

With this, one obtains the pairwise molecular scattering cross-sections as

$$\sigma_{jk}(s,\alpha,\Omega) = |g_j||g_k|\cos(\mathbf{S}\cdot\mathbf{R}_{jk} + \eta_k - \eta_j) \times \prod_\gamma \langle\psi_\gamma(q_\gamma)|\cos(\mathbf{S}\cdot\mathbf{c}_{jk,\gamma}q_\gamma)|\psi_\gamma(q_\gamma)\rangle \quad (4)$$

Here, the vector $\mathbf{R}_{jk}$ denotes the equilibrium displacement between the atoms in the molecular frame, while the vectors $\mathbf{c}_{jk,\gamma}$ give the contribution of each (mass-weighted) vibrational mode γ to the displacement from the equilibrium. The vectors $\mathbf{c}_{jk,\alpha}$ are given explicitly in terms of matrices, $\mathbf{M}$, that prescribe

the transformation from body-fixed Cartesian nuclear coordinates to normal modes, $(\mathbf{c}_{jk,\gamma})_\mu = (\mathbf{M}^{\mathrm{T}})_{k\mu,\gamma} - (\mathbf{M}^{\mathrm{T}})_{j\mu,\gamma}$ ($j, k = 1, ..., N$; $\mu = X, Y, Z$). The momentum transfer vector in the molecular frame, **S**, is defined as

$$\mathbf{S} \equiv \mathbf{U}^{\mathrm{T}}(\Omega)\cdot\mathbf{s}$$

where $\mathbf{U}(\Omega)$ is the orthogonal matrix that transforms from molecular body-fixed coordinates to laboratory coordinates.

For the calculation of diffraction patterns of *s*-tetrazine in specific vibronic eigenstates, we use the geometrical structure and normal mode displacements discussed earlier. Vibrational modes that are not excited are assumed to remain in their zero point vibrational state. Note that the displacements arising from the zero point vibrational motions are included in the product of eq 4 and lead to an overall damping of the diffraction signal at large *s*.

Having established the theoretical framework of the diffraction signature of molecules in specific eigenstates, we now turn our attention to the situation where a laser pulse excites the molecular sample through a one-photon interaction with the molecular transition dipole moment. For the calculations of the present paper we chose the pump laser to be linearly polarized along either the *x*-direction or the *z*-direction (see Figure 2). The polarized laser will preferentially excite those molecules that have transition moments parallel to the laser polarization. For example, for excitation with a *z*-polarized laser, the probability that a molecule is lifted to the excited state is proportional to $\cos^2\theta$.[24] In this case the signal with the pump laser on will be

$$I_{\mathrm{laser-on}}(s,\alpha) = \int I_{S_1,v}(\cos^2\theta)\rho(\Omega)\,\mathrm{d}\Omega + \int I_{S_0,v=0}(1-\cos^2\theta)\,\rho(\Omega)\,\mathrm{d}\Omega \quad (5)$$

while the signal with the pump laser off is simply

$$I_{\mathrm{laser-off}} = \int I_{S_0,v=0}\rho(\Omega)\,\mathrm{d}\Omega \quad (6)$$

In these expressions, ρ is the orientational distribution function for the initial molecular sample, which depends on the Euler angles Ω. For a randomly oriented sample $\rho(\theta,\varphi,\chi) = 1/8\pi^2$. The integration is over all angles, $\mathrm{d}\Omega = \sin(\theta)\,\mathrm{d}\theta\,\mathrm{d}\phi\,\mathrm{d}\chi$.

For simplicity, every molecule that interacts with the laser pulse is assumed to be excited, so the transition probability f_0 is unity. For general cases, where $f_0 \neq 1$, this f_0 factor will appear along with $\cos^2\theta$ in the above expressions. Inclusion of this factor will only rescale, but not change, the difference diffraction patterns $I_{\mathrm{laser-on}} - I_{\mathrm{laser-off}}$ that we discuss when analyzing the results.

For our assumed high-energy electron diffraction experiment, we used $k_0 = 100$ Å^{-1}, which corresponds to an incident electron energy of about 40 keV. In this case we can, to a good approximation, ignore any changes in the magnitude of the electron momentum during the scattering.

C. Molecular Alignment. Following our recent demonstration that alignment of molecules in intense laser fields can greatly enhance the modulation depth of gas-phase diffraction patterns,[5] we explore now to what extent the signatures of specific vibronic states change when the molecules are aligned. To approach this question, we follow the outline of our previous work and assume that *s*-tetrazine molecules are aligned by intense electromagnetic fields. Following the alignment scheme proposed by Friedrich and Herschbach,[25] the electromagnetic field tends to align molecules such that the axis of highest polarizability coincides with the laser field. In particular, our field defines an effective rotational Hamiltonian

$$\bar{H} = -\frac{1}{8}E_0{}^2(\alpha_{xx} + \alpha_{yy})$$

where $\alpha_{xx}(\Omega)$ and $\alpha_{yy}(\Omega)$ are the elements of the molecule's polarizability tensor in the laboratory frame, and E_0 is the magnitude of the electric field. This leads to a temperature-dependent orientational probability distribution

$$\rho(\Omega) = \sum_i |\psi_i|^2 e^{-E_i/k_BT} \Big/ \sum_i e^{-E_i/k_BT} \quad (7)$$

where $|\psi_i|^2$ is the probability density distribution arising from a specific rotational eigenstate i in the presence of the electromagnetic field.

For our calculations we followed the approach of Ref. 5 and diagonalized the effective rotational Hamiltonian to find the states ψ_i. We then evaluated eq 7 using a rotational temperature of 5 K, which is appropriate for *s*-tetrazine molecules seeded in a free jet expansion. The alignment laser is assumed to be circularly polarized, with intensities of 1.06×10^{12}, 4.25×10^{12}, and 9.56×10^{12} W/cm^2, corresponding to electric fields ($E_0/\sqrt{2} = E_{x0} = E_{y0}$) of 2×10^7, 4×10^7, and 6×10^7 V/cm.

III. Results and Discussion

A. Diffraction from Isotropic Samples. To quantify the changes in the diffraction patterns upon electronic and vibrational excitation, we separately calculate the patterns of the molecules in the ground state and in the excited state. We then consider the difference between the two patterns and divide the difference pattern by the pattern of the molecule in the ground state. The resulting fractional difference pattern can be understood as a percent change of the diffraction signal upon excitation, assuming all molecules are excited by the laser. These patterns can be directly compared to experimental data, because both the laser-excited and the ground-state patterns are experimentally measurable without a need to subtract an atomic background, as is most often done in diffraction analysis. Moreover, the ratio pattern we calculate is proportional to the experimentally measured ratio, with the proportionality coefficient just being the fraction of the molecules excited. That quantity, which is of no further interest to us, can be obtained by fitting procedures.

The transition dipole moment of the *s*-tetrazine S_0-S_1 transition is perpendicular to the plane of the aromatic ring. Excitation with a laser polarization that is directed along the electron beam propagation axis, the *z*-axis, therefore preferentially excites those molecules with the aromatic ring perpendicular to the electron beam. There is no selection with respect to the χ-angle, the angle of rotation about the transition dipole moment. Therefore, the observed diffraction patterns are cylindrically symmetric.

Figure 3 shows the difference patterns divided by the ground-state patterns, for various vibronic excitations, as a function of the projection of the scattering vector onto the plane of the detector. The top panel shows the difference between the excited-state patterns ($S_1,0^0$; $S_1,1^2$; $S_1,6a^3$; and $S_1,16a^8$) and the pattern of the ground-state molecules ($S_0,0_0$). The bottom panel plots the difference between the vibronically excited molecules (S_1,v) and the electronically only excited molecules ($S_1,0^0$).

We characterize the similarity between any two patterns, with intensities I_1 and I_0, by the value of $R(I_1,I_0)$, which is defined

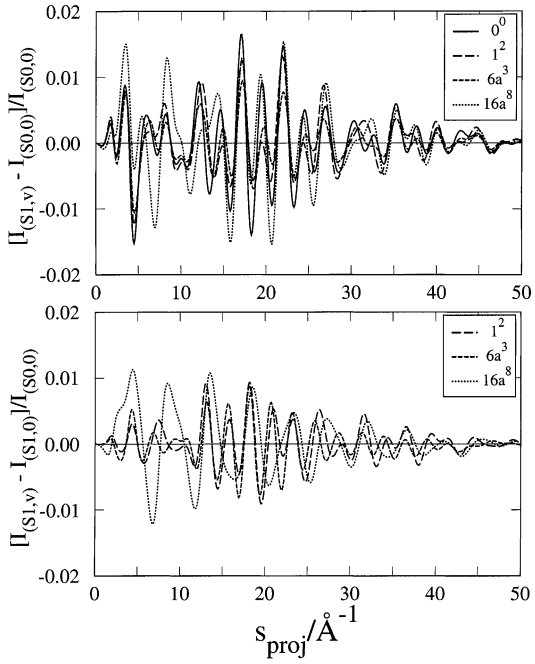

Figure 3. Diffraction signatures of *s*-tetrazine molecules excited to specific vibronic states, as indicated in the legends. The excitation laser is linearly polarized along the *z*-direction, and the molecular orientations are isotropic (before excitation). The top panel compares the vibronically excited states to the 0_0 level, while the bottom panel compares the vibrationally excited levels of the S_1 state to the vibrationless level of S_1.

as the root-mean-square deviation

$$R(I_1,I_0) = \sqrt{\left\langle\left(\frac{(I_1 - I_0)}{\left(\frac{1}{2}\right)(I_1 + I_0)}\right)^2\right\rangle} \qquad (8)$$

The average is over all the calculated values of *s*, which in our calculations stretch from $s_{proj} = 0$ Å^{-1} to $s_{proj} = 50$ Å^{-1}. The values of *R* depend slightly on the somewhat arbitrary cutoff value. Even so, the *R*-values serve as a useful quantitative measure for the agreement between any pair of patterns.

The solid line, in the top panel of Figure 3, depicts the fractional change of the diffraction signal when the molecule undergoes a transition between the vibrational ground states of S_0 and S_1. The *R*-value of that trace is calculated to be 0.0048. From the plot it is seen that the signal oscillates about zero with a variable amplitude, with typical displacements of 0.01, up to $s \approx 30$ Å^{-1}. This implies that the diffraction pattern changes by about ±1% when excited to the electronically excited state. This magnitude is not surprising, as it reflects the magnitude of the changes in the internuclear distances when the molecule is electronically excited.

The other three lines in the top panel of Figure 3, and the three traces in the bottom panel, refer to the fractional difference patterns of the different vibronic states, as indicated in the legends. The magnitudes of the oscillations are again in the 1% range, and the *R*-values are in the order of 0.003−0.005. A matrix of *R* values between all the traces is given in Table 3. Several important points are evident from Figure 3 and Table 3. First, the diffraction patterns of specific vibronic states exhibit characteristic features that are distinct from that of the purely electronically excited level. Second, the magnitude of those features is about the same as that for the electronic excitation only, on the order of ±1%. While clearly the vibronically excited levels have wave functions that are centered about the equilibrium geometry of the S_1 state, the characteristic signature of the diffraction patterns reveals that it is the vibrational probability density distribution, rather than the equilibrium geometry, that gives these diffraction patterns their unique shapes. Third, even though the vibrational motions along coordinates 1 and 6a are fairly similar, their diffraction signatures are quite distinct.

TABLE 3: Changes in Diffraction Patterns with Vibrational Excitation of the S_1 State[a]

0_0	0^0	1^2	$6a^3$	$16a^8$	
0	0.0048	0.0041	0.0029	0.0055	0_0
	0	0.0028	0.0026	0.0043	0^0
		0	0.0019	0.0045	1^2
			0	0.0047	$6a^3$
				0	$16a^8$

[a] Shown here are the *R* values, calculated using eq 8, with I_0 and I_1 taken as the diffraction traces for the row and column vibronic states, respectively.

The most important conclusion drawn from Figure 3 and Table 3 is that the individual vibrational motions of a polyatomic molecule give rise to specific diffraction signatures. Neither the presence of the many vibrational motions of the polyatomic molecule nor the averaging over all orientations of the molecules in the isotropic sample washes out the signature of vibrational excitation. The magnitude of the changes, while small, is well within the reach of existing electron diffraction instruments.

When the polarization of the pump laser is *perpendicular* to the electron beam, the electronic excitation preferentially selects those molecules whose aromatic planes are aligned with the electron beam propagation direction. As a result, the diffraction patterns are asymmetric with respect to rotation about the electron beam axis. Figure 4 displays difference diffraction patterns for excitation to the vibronic states 0^0, 1^2, $6a^3$, and $16a,^8$ by a laser that is linearly polarized along the *x*-direction. In these contour plots the intensity of the signal, defined again by the ratio of the difference between the pump-laser-on and the pump-laser-off patterns, divided by the pump-laser-off pattern, is encoded by the color as indicated by the color bars. The difference signal is plotted against the magnitude of the projection of the **s**-vector (ordinate) and the rotation α about the *x*-axis (abscissa). Only one quadrant is displayed; the others are symmetrically equivalent.

The diffraction patterns of Figure 4 show again that each vibronically excited state gives rise to a characteristic diffraction signature. All patterns show a strong modulation in the $\alpha = 90°$ direction, the direction in which the molecular planes are preferentially aligned. In addition, the $16a^8$ out-of-plane vibration leads to a significant modulation along the $\alpha = 0°$ direction. The intensity change observed in the difference diffraction patterns is again in the 1% range, depending on the magnitude and direction of the scattering vector.

For the noncylindrically symmetric patterns of Figure 4, the *R*-values defined by eq 8 depend on the angle α. Figure 5 shows this dependence for the different vibronic states examined. It is again clear that the different vibronic states have quite distinct diffraction signatures. Qualitatively, the in-plane vibrations are characterized by a large *R*-value in that direction where the molecular plane is preferentially aligned, i.e., $\alpha = 90°$. This characteristic trait is shared with the effect of the purely electronic excitation, in which *s*-tetrazine changes its structure within the plane of the aromatic ring only. The 16a out-of-plane vibration, however, has maxima in *R* both along the plane of the ring ($\alpha = 90°$) and perpendicular to the ring ($\alpha = 0°$). Therefore, even a qualitative difference diffraction image, where

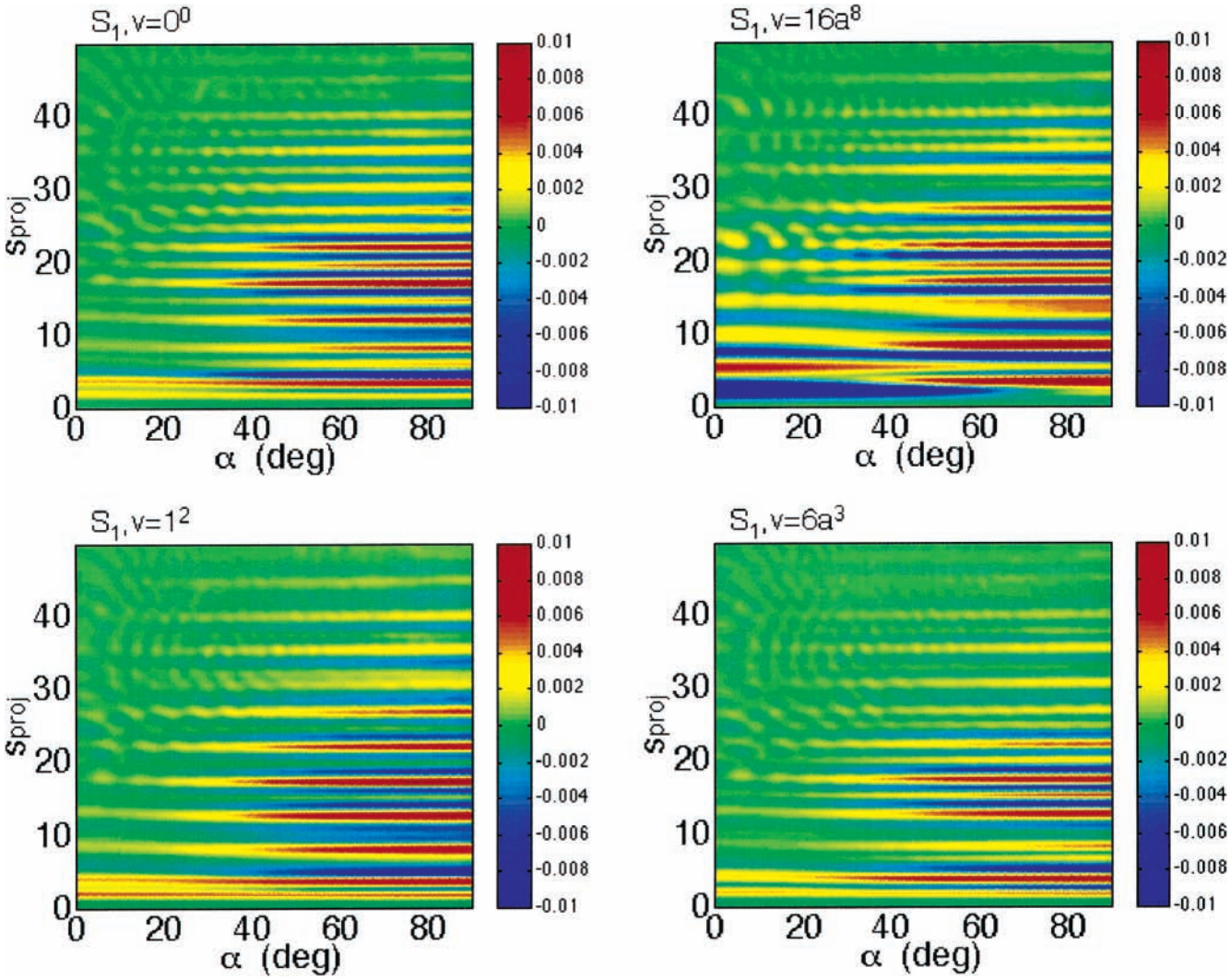

Figure 4. Difference diffraction patterns for *s*-tetrazine molecules excited to specific vibronic states, as labeled, by an excitation laser that is linearly polarized in the *x*-direction, i.e., perpendicular to the electron beam propagation direction. The abscissa is the rotation about the electron beam axis, and the ordinate is the projection of the **s**-vector onto the detector, measured in $Å^{-1}$.

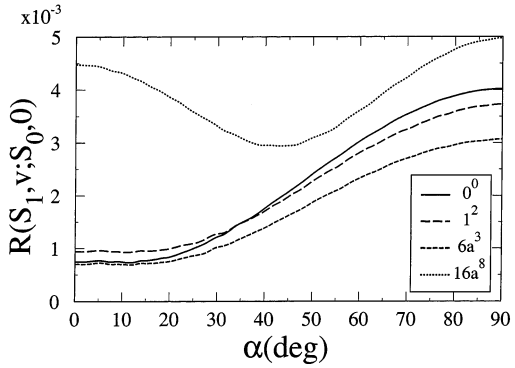

Figure 5. *R*-values, as defined by eq 8, as a function of the detector angle α, for the diffraction patterns of Figure 4. The *R*-value is a measure for the dissimilarity of the excited-state pattern compared to the pattern of the ground state, $S_0,0_0$.

all α directions are mapped simultaneously, can reveal the vibrational motion of a particular vibrational state.

B. Diffraction from Aligned Samples. Alignment of molecules in high-intensity laser fields can tremendously increase the modulation depth of the diffraction patterns, rendering the molecular component of the patterns much more readily observable.[5] An interesting question to explore in the present context is therefore if the specific signatures of individual vibronic states can be similarly enhanced using the alignment technique. Figure 6 exemplifies the achievable enhancement by comparing the diffraction signatures of two vibronic levels, 0^0 and $6a^3$, for alignment intensities of 0 and 4.25 TW/cm^2. It is apparent that the alignment increases the modulation depth by about 1 order of magnitude. Given that the vibrational signatures are only in the 1% range, this enhancement is quite appreciated by experimentalists.

A potential concern is that the patterns of aligned molecules can differ from those of randomly oriented molecular samples.[5] In the context of the present discussion, we are therefore interested in exploring the following two questions: First, does the vibrational signature persist in the diffraction patterns as the molecules are aligned, and can we selectively enhance or suppress the signature of the vibrational excitation? And, second, does the dependence of the shape of the difference patterns on the vibrational excitation dominate over the variability of the diffraction patterns with the alignment laser intensity? An affirmative answer to the first question is obviously necessary for alignment experiments to be useful for the purpose of measuring vibrational diffraction patterns. The second question is important because the intensity of the alignment laser may have some variation over the volume of probed molecules. Any

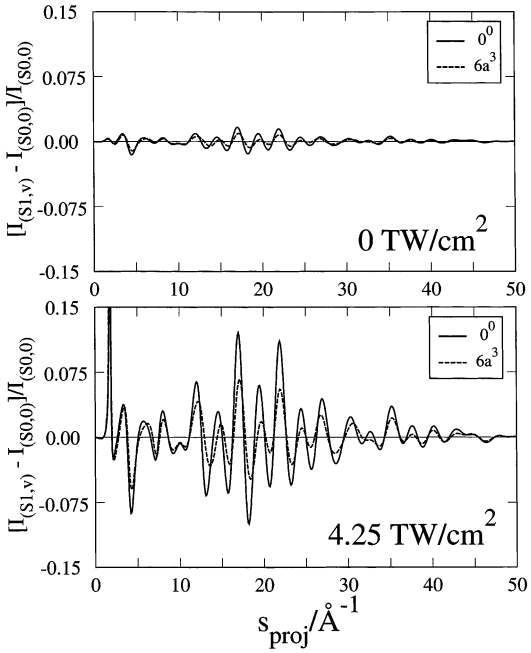

Figure 6. Difference diffraction signals of *s*-tetrazine excited to S_1 levels 0^0 and $6a^3$, with a *z*-polarized laser beam. The top panel is for isotropic molecules, while the bottom panel corresponds to molecules aligned using an alignment laser intensity of 4.25 TW/cm^2. Both panels are plotted on the same vertical scale to illustrate the enhancement of the modulation depth achieved by the alignment of the molecules.

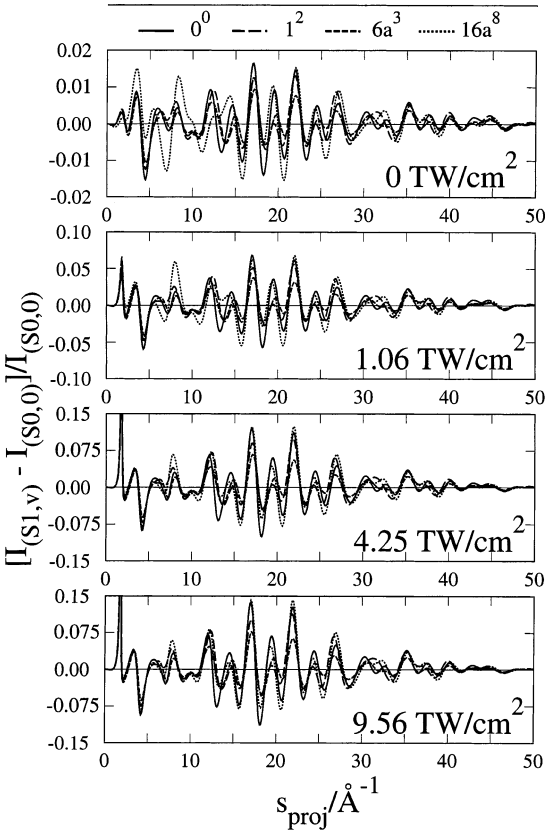

Figure 7. Difference diffraction signals of the excited-state molecules vs the ground-state molecules, for specific vibronic states as indicated. The excitation laser is linearly polarized along the *z*-direction, and the molecules are aligned in the (*x*,*y*) plane by a circularly polarized laser with an intensity as labeled. Note the differences in the scales between the panels.

change in the shape of the diffraction signal should be small compared to the change induced by the vibrational excitation.

We first discuss the fractional pump−probe difference patterns for the case of an alignment laser that is circularly polarized in the (*x*,*y*) plane. In this case the diffraction patterns are again cylindrically symmetric. Figure 7 shows, for excitation with a *z*-polarized excitation laser, the difference patterns for all the vibronic states, for alignment intensities of 0, 1.06, 4.25, and 9.56 TW/cm^2. (The data of Figure 6 are included in this plot.) Plotted is the difference between the excited-state patterns (S_1, $v = 1^2$, $6a^3$, and $16a^8$), and the ground-state pattern, (S_0, $v = 0$), divided by the signal of the ground-state patterns. From Figures 6 and 7 we conclude that the fractional difference patterns do remain sensitively dependent on the vibrational excitation at all alignment intensities. As was previously observed for the molecules in the ground state,[5] the modulation depth increases dramatically when the molecules are aligned by intense laser fields.

To characterize the difference between the excited-state patterns and the ground-state patterns, we again calculate the *R* values, defined by eq 8. The values for the four different vibrational states, and the alignment laser intensities from 0 to 9.56 TW/cm^2, are listed in Table 4. It is seen that even an alignment intensity of 1 TW/cm^2 increases the modulation depth by about a factor of 4. Raising the intensity to 9.56 TW/cm^2 increases this factor to about 10. Hence, as we noted, alignment of the molecules significantly improves the signature of the vibrational excitation in the diffraction fringes.

To investigate the relative sensitivity of the difference diffraction patterns toward vibronic excitation on one hand, and the alignment laser intensity on the other hand, it is necessary to define a new metric that characterizes the similarity of difference diffraction patterns. (The *R*-values, as defined in eq 8, diverge if I_1 and I_0 are difference diffraction signals, rather than total signals, since the difference signals have nodes.) We chose as a measure for the similarity the simple root-mean-

TABLE 4: Changes in Diffraction Patterns as a Function of Alignment Laser Intensity[a]

	0^0	1^2	$6a^3$	$16a^8$
isotropic	0.0048	0.0041	0.0029	0.0055
1.06 TW	0.019	0.017	0.012	0.021
4.26 TW	0.035	0.034	0.027	0.037
9.56 TW	0.039	0.038	0.030	0.041

[a] Shown here are the values of *R*, as defined in eq 8, with I_0 computed from the ground electronic and vibrational states and I_1 from the S_1 vibronic states listed.

square deviation between two difference patterns. As a reference difference pattern, we take that of the partially clamped molecules, with orientations $\theta = 0°$ and $\phi = 0°$. As neither the alignment laser nor the excitation polarization significantly affects the χ angle, we use as a reference state the one where χ is averaged over all values. However, the absolute value of the root-mean-square deviation between two difference patterns is a meaningless quantity. We therefore reference all values to that of the $S_1,0^0 - S_0,0_0$ difference pattern, for the isotropic sample. Thus, we characterize the dimensionless similarity S_i of two difference diffraction patterns by the quantity

$$S_i = \frac{\sqrt{\langle (I_i - I_0)^2 \rangle}}{\sqrt{\langle (I_1 - I_0)^2 \rangle}} \tag{9}$$

where I_0 refers to the $0^0 - 0_0$ difference pattern of the partially clamped molecules, I_1 is the $0^0 - 0_0$ difference pattern of the isotropic sample, and I_i is the difference diffraction pattern for the vibronic excitation to be examined.

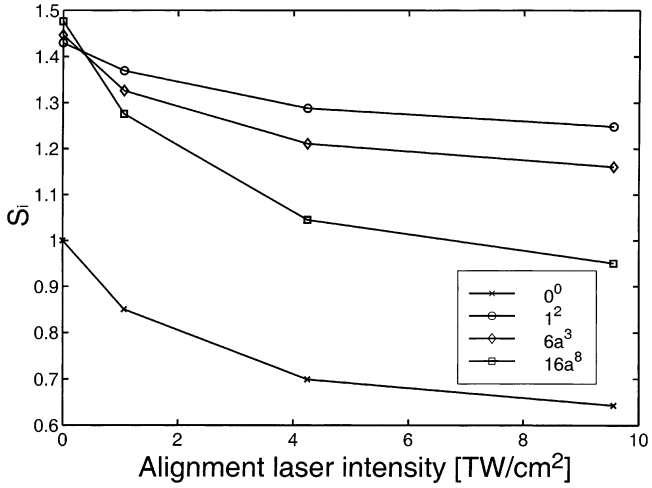

Figure 8. S_i-values, as defined by eq 9, for pump−probe diffraction patterns of different vibronically excited states, as labeled in the legend, as a function of the alignment laser intensity. S_i measures the similarity of two pump−probe difference diffraction patterns; smaller values of S_i indicate that two patterns are more similar to each other.

The S_i values of the investigated vibronic states are plotted in Figure 8. For the 0^0 state, the values for different alignment intensities fall on a smoothly decaying curve between the reference value for isotropic samples, 1, and the reference value for the partially clamped molecules, 0. That value would be reached at infinitely large alignment laser intensities. We note that the first 1.06 TW/cm^2 causes a rapid change of the pattern but that the effect levels off at higher alignment intensities. This behavior has already been described previously.[5]

Figure 8 also shows that, at all alignment intensities, the S_i values of the vibrationally excited states are larger than those of the 0^0 level. This suggests that these patterns retain a distinct shape at all levels of the alignment laser intensity. The dissimilarities (as characterized by changes in the S_i values) induced by reasonably small changes in the alignment intensity are much smaller than those arising from the vibrational excitation, in particular at the high alignment intensities. We conclude that the vibrational excitation remains distinct and observable even in the presence of small variations of the alignment intensity.

C. Example of Using Diffraction To Map Vibrational Wave Functions. An important observation relates to the vibration 16a. This observation illustrates the kind of analysis that the pump−probe diffraction technique allows us to perform. In essence, the technique provides a vector correlation between the direction of the vibrational motion and the face of the molecule selected by the alignment laser. This kind of correlation is precisely what we need to obtain directional information on the vibrational dynamics of the molecule.

For isotropic samples, the diffraction pattern of the $16a^8$ vibration has the most distinctive shape, as evidenced by a large S_{16a^8} value. On the other hand, as the molecules are aligned by the laser field, the distinctiveness of the diffraction signature disappears, and at the highest level of alignment the vibration $16a^8$ actually has the lowest value of S_i among all the vibrationally excited states. Apparently, the unique shape of the $16a^8$ vibrational diffraction pattern disappears as the molecules are aligned in the field.

Figure 9 traces the loss of this characteristic shape through the levels of alignment intensity. Plotted at the different alignment intensities are the fractional difference patterns for $16a^8$ excitation, as well as the pattern for 0^0 excitation for the

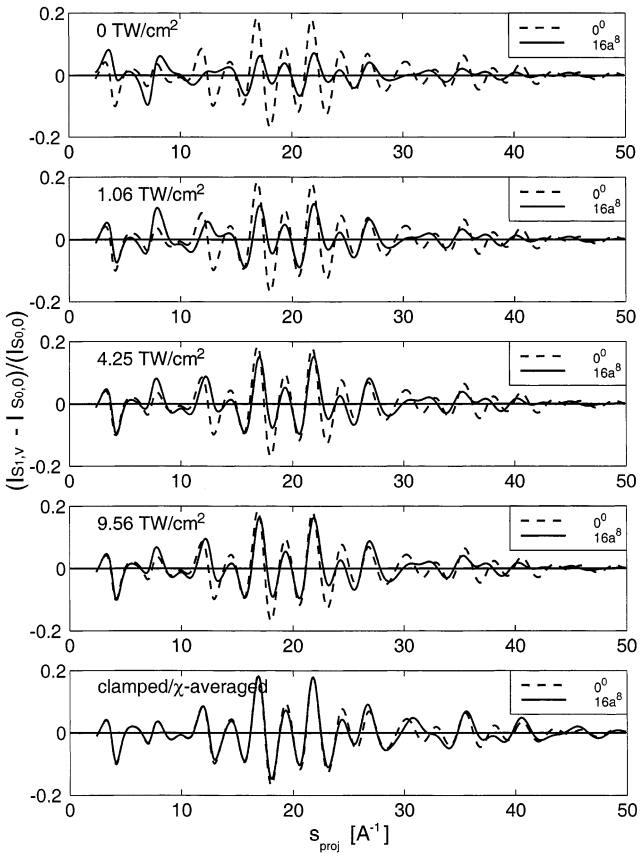

Figure 9. Difference diffraction signals of the excited-state molecules vs the ground-state molecules, for the $16a^8$ and the 0^0 states. The excitation laser is linearly polarized along the *z*-direction, and the molecules are aligned in the (*x*,*y*) plane by a circularly polarized laser with an intensity as labeled.

reference case of θ- and ϕ-clamped/χ-averaged molecules. To illustrate the convergence of the shapes of the two fractional difference patterns in the presence of the different modulation depths arising from the alignments, the $16a^8$ trace in each panel was scaled such that the *R*-value between it and the 0^0 trace is minimized. It is clearly seen that while for isotropic samples the vibration has a diffraction pattern very distinct from that of the ground vibrational state, this difference is lost as the molecules are aligned. In the limit of the clamped molecule, the pattern of the $16a^8$-excited molecules becomes almost identical to the unexcited molecule, especially for diffraction angles below 30 Å^{-1}.

To further explore the remarkable diffraction signature of the $16a^8$ vibration, we examine its dependence on the alignment, using the geometry where the aromatic rings are aligned in the (*y*,*z*) plane. Those diffraction images depend again on the orientation α about the electron beam axis. Figure 10 depicts the fractional difference patterns of the $16a^8$ and the 0^0 vibrations, each for the case of alignment by a 9.56 TW/cm^2 field and for the case of clamped/χ-averaged molecules. At $\alpha = 90°$, in the plane of the aromatic ring, the diffraction signature of the vibrational motion disappears, and the pattern of the vibrationally excited molecule approaches that of the molecule without vibrational excitation. This is quite like the previous observation on the (*x*,*y*) aligned molecules. However, at smaller values of α, the patterns of the vibrationally excited molecules look quite different from those of the vibrationless molecule. At $\alpha = 0°$ the vibrationless molecule has only a very weakly modulated pattern. In contrast, the pattern of the $16a^8$ vibration is strongly modulated along the $\alpha = 0°$ direction. Clearly, the

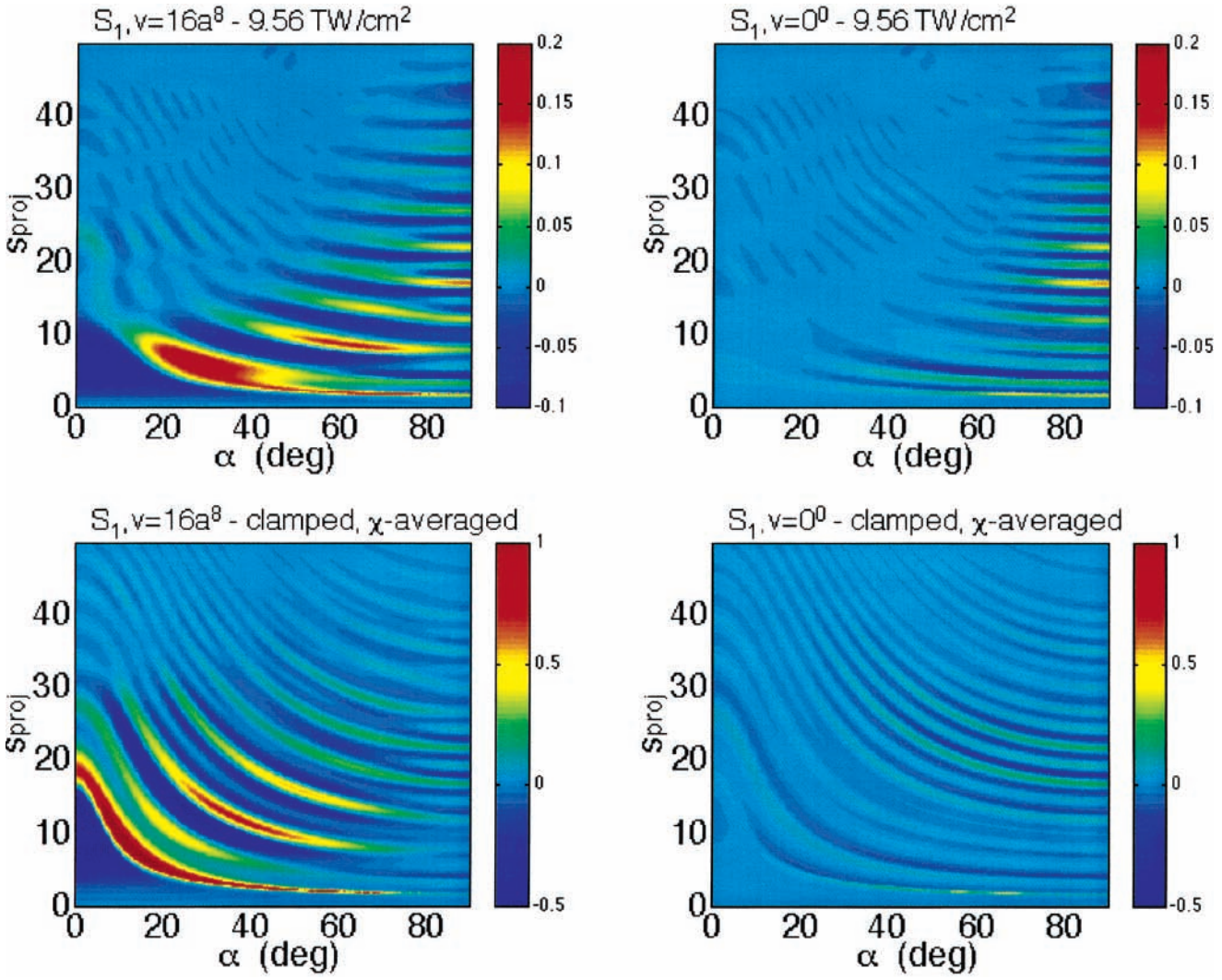

Figure 10. Difference diffraction signals of the excited-state molecules vs the ground-state molecules, for the $16a^8$ and the 0^0 states. The excitation laser is linearly polarized along the *x*-direction. In the top panels, the molecules are aligned in the (*y*,*z*) plane by a circularly polarized laser with an intensity of 9.56 TW/cm^2. In the bottom panels the molecules are clamped at the (θ, ϕ) = (90°, 0°) position, while χ is averaged over all angles.

vibrational diffraction pattern of this vibration is very sensitive to the respective orientation of the electron beam and the aromatic ring.

The sensitivity of the vibrational diffraction signatures to the orientation of the molecular plane with respect to the electron beam, and the direction of observation on the detector, can be understood qualitatively by a consideration of the geometrical displacement vectors of the vibrational motion and the geometry of the diffraction experiment. Reducing the problem to a simple scheme, Figure 11 illustrates the dependence of the diffraction fringes arising from scattering off two-point sources as a function of the relative positions of points. When the two points are aligned with the incoming electron beam (top panel), the resulting diffraction pattern is very sensitive toward the alignment of the points: the fringes change rapidly with the angle β. On the other hand, if the two points are positioned at a large angle to the incoming electron beam (lower panels), the diffraction patterns are quite insensitive toward changes in the angle of orientation.

Figure 12 applies this insight to the 16a vibration of the *s*-tetrazine molecule. The displacement of any pair of atoms during the vibration corresponds qualitatively to a change in the angle β of the two-point model. When the aromatic ring is perpendicular to the electron beam (top panel), the vibrational displacement moves the atoms almost parallel to the electron beam; this corresponds to the situation in Figure 11 with β close to 90°. In this case, the diffraction pattern is fairly insensitive to the motion of the atoms, explaining the similarity of the $16a^8$ and the 0^0 diffraction patterns seen at high alignment intensities in Figure 9. Moreover, we understand that better alignment leads to more similar patterns, in agreement with Figure 9.

If the ring of the aromatic molecule is aligned in the (*y*,*z*) plane (Figure 12, bottom panel), the 16a vibrational motion moves the atoms out of the plane of the molecule, about parallel to the s_x ($\alpha = 0°$) axis. For scattering along $\alpha = 0°$, the situation corresponding to the case where $\beta \approx 0°$ in Figure 11a. This explains the strong dependence on the vibrational motion seen in Figure 10 for small α. On the other hand, for large α, the vibrational motion is perpendicular to the electron scattering, making for a negligibly small effect of the vibration on the diffraction pattern in that direction. In Figure 10 we see that at large α, there is indeed very little change in the diffraction pattern upon vibrational excitation.

Opposite arguments apply to the vibrations 1^2 and $6a^3$. The displacement vectors are now similar to bond-stretching motions for a two-point scatterer. Those displacements are prominently seen when the atoms are perpendicular to the electron beam and hardly observed when the points align with the electron beam. As a result, for the case of (*x*,*y*)-aligned *s*-tetrazine molecules, the diffraction patterns are very sensitive to the

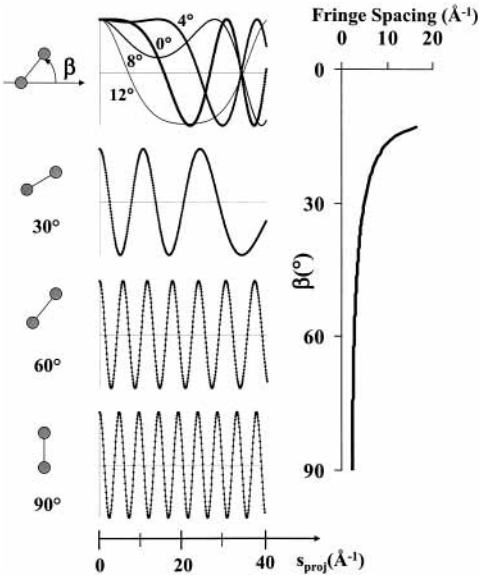

Figure 11. Dependence of the diffraction signal of a two-point scatterer on its alignment with respect to the electron beam (arrow). For very small values of the angle β, the diffraction signal is very sensitive toward small changes of β. At large values of β, the sensitivity of the diffraction signal on β becomes very small.

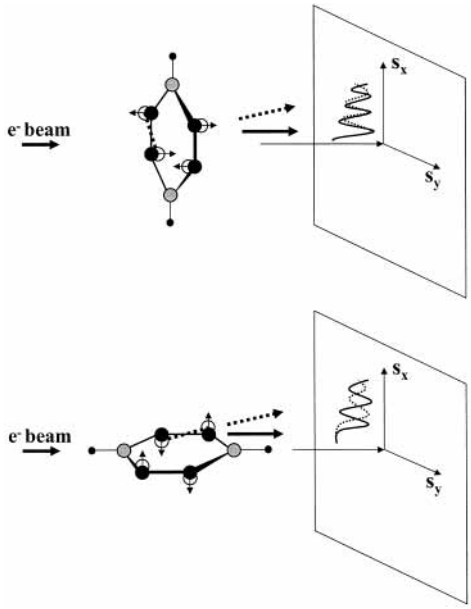

Figure 12. Schematic illustration of the vibrational displacements of the atoms during the 16a vibration, and their effects on diffraction signals for the two different orientations of the *s*-tetrazine molecule.

vibrational motions in all detector directions α. For (y,z)-aligned molecules there is a strong dependence when the diffraction patterns are observed along $\alpha = 90°$, that is, along the plane of the aromatic ring. It is in this direction that the vibrational motions have their displacements. However, the dependence of the diffraction pattern on the vibrational excitation in modes 1 and 6a is extremely small when the diffraction pattern is observed along the $\alpha = 0°$ direction.

IV. Summary

In this paper we have shown that the probability density distributions of vibrational wave functions in polyatomic molecules in the gas phase are observable by electron diffraction. The effect of the vibrational excitation is in the range of 1% of the total signal over significant parts of the diffraction image for isotropic samples, and much larger for aligned samples. This is well within the reach of present day pump−probe diffraction instruments. Even with isoenergetic vibrations, the vibrational diffraction patterns are sensitive to the specific vibrational motion. Not only can one discern obviously different vibrational geometries, such as in-plane and out-of-plane vibrations, one can easily distinguish vibrations of the same symmetry. The origin of the effect is that the diffraction image of the vibrational motion is sensitive to the orientation of the molecule with respect to the electron beam and the geometry of the scattering process. Using different geometries of the detector angle, the polarization of the pump laser, and the orientation of the alignment laser, the diffraction signatures of different vibrational motions can be selectively enhanced.

The presented work opens the door to a new type of investigation into molecular vibrations. The imaging of vibrational motions using different geometries may allow for the development of a tomography whereby the three-dimensional structure of the wave function is directly observed using diffraction. Such an experiment could have vastly more information content than a typical one-dimensional spectrum, which measures a scalar quantity. This information could be used, for example, to unambiguously identify molecular vibrations that are sometimes difficult to assign. Alternatively, it may be possible to observe the flow of energy through the vibrational phase space by observing the diffraction patterns associated with vibrational wave packets—which requires only that time resolution is added to the pump−probe diffraction experiment.

Acknowledgment. This work is supported by the Army Research Office under Contracts DAAD19-00-0141 and DAAD19-03-1-0140, the Chemical Sciences, Geosciences and Biosciences Division, Office of Basic Energy Sciences, Department of Energy, Grant No. DE-FG02-03ER15452, and by the National Science Foundation (NSF) under Grants CHE-0131114 and CHE-0212823.

References and Notes

(1) *Time-Resolved Diffraction*; Helliwell, J. R., Rentzepis, P. M., Eds.; Clarendon Press: Oxford, U.K., 1997.

(2) Cao, J.; Ihee, H.; Zewail, A. H. *Proc. Natl. Acad. Sci. U.S.A.* **1999**, *96*, 338. Ruan, C.-Y.; Lobastov, V. A.; Srinivasan, R.; Goodson, B. M.; Ihee, I.; Zewail, A. H. *Proc. Natl. Acad. Sci. U.S.A.* **2001**, *98*, 7117.

(3) Dudek, R. C.; Weber, P. M. *J. Phys. Chem. A* **2001**, *105*, 4167.

(4) Ryu, S.; Weber, P. M.; Stratt, R. M. *J. Chem. Phys.* **2000**, *112*, 1260.

(5) Ryu, S.; Stratt, R. M.; Weber, P. M. *J. Phys. Chem.* A **2003**, *107*, 6622.

(6) Böwering, N.; Volkmer, M.; Meier, C.; Lieschke, J.; Fink, M.; *Z. Phys. D: At., Mol. Clusters* **1994**, *30*, 177. Böwering, N.; Volkmer, M.; Meier, C.; Lieschke, J.; Dreier, R. *J. Mol. Struct.* **1995**, *348*, 49.

(7) Ben-Nun, M.; Martinez, T. J.; Weber, P. M.; Wilson, K. R. *Chem. Phys. Lett.* **1996**, *262*, 405.

(8) Geiser, J. D.; Weber, P. M. *J. Chem. Phys.* **1998**, *108*, 8004.

(9) Ischenko, A. A.; Ewbank, J. D.; Schäfer, L. *J. Phys. Chem.* **1995**, *99*, 15790. Ewbank, J. D.; Schäfer, L.; Ischenko, A. A. *J. Mol. Struct.* **2000**, *524*, 1.

(10) Innes, K. K.; Franks, L. A.; Merer, A. J.; Vermulapalli, G. K.; Cassen, T.; Lowery, J. *J. Mol. Spectrosc.* **1977**, *66*, 465.

(11) Brumbaugh, D. V.; Haynam, C. A.; Levy, D. H. *J. Mol. Spectrosc.* **1982**, *94*, 316.

(12) Hochstrasser, R. M.; King, D. S. *J. Am. Chem. Soc.* **1975**, *97*, 4760. Hochstrasser, R. M.; King, D. S.; Smith, A. B. *J. Am. Chem. Soc.* **1977**, *99*, 3923.

(13) Scheiner, A. C.; Schaefer, H. F., III *J. Chem. Phys.* **1987**, *87*, 3539.

(14) Zhao, X.; Miller, W. B.; Hintsa, E. J.; Lee, Y. T. *J. Chem. Phys.* **1989**, *90*, 5527. Nahon, L.; Morin, P.; Larzilliere, M.; Nenner, I. *J. Chem. Phys.* **1992**, *96*, 3628.

(15) Stanton, J. F.; Gauss, J. *J. Chem. Phys.* **1996**, *104*, 9859.

(16) Stanton, J. F.; Gauss, J.; Watts, J. D.; Nooijen, M.; Oliphant, N.; Perera, S. A.; Szalay, P. A.; Lauderdale, W. J.; Gwaltaney, S. R.; Beck, S.; Balková, A.; Bernholdt, D. E.; Baeck, K. K.; Rozyczko, P.; Sekino, H.; Hober, C.; Bartlett, R. J. *Advanced Concepts in Electronic Structure Theory (ACES II)*, program; Quantum Theory Project, University of Florida: Gainesville, FL. Integral packages included are: VMOL (J. Almöf and P. R. Taylor); VPROPS (P. R. Taylor); ABACUS (T. Helgaker, H. J. Aa. Jensen, P. Jorgensen, J. Olsen, and P. R. Taylor).

(17) Baeck, K. K.; Watts, J. D.; Bartlett, R. J. *J. Chem. Phys.* **1997**, *107*, 3853. Baeck, K. K. *J. Chem. Phys.* **2000**, *112*, 1.

(18) Dunning, T. H., Jr. *J. Chem. Phys.* **1970**, *53*, 2823.

(19) Redmon, L. T.; Purvis, G. D., III; Bartlett, R. J. *J. Am. Chem. Soc.* **1979**, *101*, 2856. The exponent value of polarization functions for the hydrogen atom has been obtained by averaging the two tabulated values.

(20) Job, V. A.; Innes, K. K. *J. Mol. Spectrosc.* **1978**, *71*, 299.

(21) Depending on the character of a vibrational mode, the frozen-core effects of the drop-MO method may result in a bigger-than-average error. Such an error, 8%, was found between our value of the S_1-state 6b vibrational mode, 259.3 cm^{-1}, and the value of Ref. 15, 281 cm^{-1}.

(22) Mott, N. F.; Massey, H. S. W. *The Theory of Atomic Collisions*, 2nd ed.; Oxford: Oxford, U.K., 1949; pp 47−49.

(23) *International Tables for Crystallography*; Wilson, A. J. C., Ed.; Kluwer Academic: Dordrecht, The Netherlands, 1991; Vol. C.

(24) Zare, R. N.; Herschbach, D. R. *Proc. IEEE* **1963**, *51*, 173.

(25) Friedrich, B.; Herschbach, D. *J. Phys. Chem.* **1995**, *99*, 15686.